Available online at www.sciencedirect.com
SCIENCE DIRECT
Journal of Solid State Chemistry 179 (2006) 2534–2540
JOURNAL OF SOLID STATE CHEMISTRY
www.elsevier.com/locate/jssc

A series of borate-rich metalloborophosphates $Na_2[M^{II}B_3P_2O_{11}(OH)]\cdot 0.67H_2O$ (M^{II} = Mg, Mn, Fe, Co, Ni, Cu, Zn): Synthesis, structure and magnetic susceptibility

Tao Yang[a], Guobao Li[a], Jing Ju[b], Fuhui Liao[a], Ming Xiong[c], Jianhua Lin[a,*]

[a]Beijing National Laboratory for Molecular Sciences, State Key Laboratory of Rare Earth Materials Chemistry and Applications, College of Chemistry and Molecular Engineering, Peking University, Beijing 100871, PR China
[b]Physics Department, Graduate School of Science, Tohoku University, Sendai 980-8578, Japan
[c]China University of Geoscience, X-ray Laboratory, Beijing 100083, PR China

Received 3 March 2006; received in revised form 5 April 2006; accepted 8 April 2006
Available online 13 May 2006

Abstract

A series of metalloborophosphates $Na_2[M^{II}B_3P_2O_{11}(OH)]\cdot 0.67H_2O$ (M^{II} = Mg, Mn, Fe, Co, Ni, Cu, Zn) have been prepared hydrothermally and their structures have been solved by single-crystal diffraction techniques. They all crystallize in a hexagonal space group $P6_3$ and form a 3D microporous structure with 12-membered ring channels consisted of octahedral ($M^{II}O_6$), tetrahedral (BO_4, PO_4) and triangular ($BO_2(OH)$) units, in which the counter Na^+ cations and water molecules are located. The Na^+ cations are mobile and can be exchanged by Li^+ in a melt of $LiNO_3$. Their open frameworks are thermal stable up to about 500 °C. Completed solid solutions between two different transition metals can also be obtained. Magnetic properties of $Na_2[M^{II}B_3P_2O_{11}(OH)]\cdot 0.67H_2O$ (M^{II} = Mn, Co, Ni, Cu) have been investigated.

Keywords: Borophosphate; Hydrothermal; Structure; Magnetic; Open framework

1. Introduction

Borophosphates have attracted considerable interests since the last decade for their potential applications as redox catalysts, molecular sieves and ion exchangers [1,2]. Transition metal atoms may incorporate into borophosphate framework as either tetrahedral or octahedral species to form metalloborophosphates, such as $A[ZnBP_2O_8]$ ($A = NH_4$, K, Rb, Cs) [3,4], $M^IM^{II}(H_2O)_2[BP_2O_8]\cdot H_2O$ (M^I = Na, K; M^{II} = Mg, Mn, Fe, Co, Ni, Zn) [5], $Fe(H_2O)_2[BP_2O_8]\cdot H_2O$ [6]. In general, the polyhedra (octahedra, tetrahedra and triangles) in metalloborophosphates share corners in the frameworks and furthermore, tend to alternatively be linked to avoid accumulation of the local charges [7–14]. An interesting observation is that the 3D microporous metalloborophosphates known so far are all phosphate rich with B:P ratio not larger than 1. A few known borate-rich borophosphates are all 1D chain structures [15–18]. In this paper, we report a new series of borate-rich metalloborophosphates $Na_2[M^{II}B_3P_2O_{11}(OH)]\cdot 0.67H_2O$ (M^{II} = Mg, Mn, Fe, Co, Ni, Cu, Zn). They are all isostructural to each other and crystallize in a 3D open framework structure consisting of $M^{II}O_6$ octahedra, BO_4/PO_4 tetrahedra and BO_3 triangles.

2. Experimental section

2.1. Materials and analysis

All reagents were of analytical grade and used as obtained from commercial sources without further purification. The chemical analysis was carried out by ICP method on an ESCALAB2000 analyzer. The thermal stability of the samples was analyzed with thermogravimetric analysis (TG) and differential thermal analysis

*Corresponding author. Fax: +8610 62751708.
E-mail address: jhlin@pku.edu.cn (J. Lin).

0022-4596/$ - see front matter © 2006 Elsevier Inc. All rights reserved.
doi:10.1016/j.jssc.2006.04.052

(DTA) on a Dupont 951 thermogravimetric analyzer in air with a heating rate of 10 °C/min from 30 to 800 °C, which provides the information about disengaged water and decomposition temperatures. The magnetic measurements were carried out on a superconducting quantum interference device magnetometer (SQUID, Quantum Design Co.) in the temperature range from $T = 2$ to 140 K. The magnetization curves were measured at 2 K up to an applied field of 7 T. The samples were grinded into fine powder and then pressed into a troche with a diameter of 6.0 mm and a thickness of 2.0 mm. The troche is fixed in a sample holder of a straw. Powder X-ray diffraction data were collected at room temperature on a Rigaku D/Max-2000 with a CuK_α radiation ($\lambda = 1.5406$ Å) from a rotating anode. Tube voltage and current were, respectively, 40 kV and 100 mA.

2.2. Preparation of $Na_2[M^{II}B_3P_2O_{11}(OH)]\cdot 0.67H_2O$ (M^{II} = Mg, Mn, Fe, Co, Ni, Cu, Zn)

The title compounds were synthesized under hydrothermal conditions. 5 mmol $M^{II}(CH_3COO)_2\cdot H_2O$ (M^{II} = Mn, Co, Ni, Cu or Zn), or $Mg(NO_3)_2\cdot 2H_2O$, or $FeSO_4\cdot 7H_2O$, and 3 mL concentrated H_3PO_4 (14.6 mol/L) and 20 mmol $Na_2B_4O_7\cdot 10H_2O$ were charged into a 50 mL Teflon reactor, and heated at 200 °C for 4 days. After cooling to room temperature, the solid products were washed extensively with hot water (80 °C) until the soluble components were completely removed. The obtained single crystals are hexagonal prisms and colorless for Mg, Mn and Zn, light yellow for Fe, purple for Co, yellow for Ni and sky-blue for Cu. The yield of the product is about 95% according to transition metal.

2.3. Crystallographic studies

Crystals of title compounds of about $0.2\times 0.2\times 0.5\,mm^3$ were used for single-crystal diffraction data collection at 293 K on a Bruker SMART X-ray diffractometer, equipped with an APEX-CCD area detector and using graphite monochromated MoK_α radiation ($\lambda = 0.71073$ Å). The data absorption correction was applied based on symmetry-equivalent reflections using the ABSOR program [19]. The structure was solved by direct method (SHELXS97) and refined by full-matrix least-squares refinement [20]. The crystal structures of $Na_2[M^{II}B_3P_2O_{11}(OH)]\cdot 0.67H_2O$ (M^{II} = Mg, Mn, Fe, Co, Ni, Cu, Zn) were determined in the hexagonal space group $P6_3$ with the structure parameters listed in Table 1. Further details on the investigations of the crystal structures may be obtained from the Fachinformationszentrum Karlsruhe, 76344 Eggenstein-Leopoldshafen, Germany (fax: +49 7247 808 666; e-mail: crysdata@fiz-karlsruhe.de), on quoting the depository numbers CSD-415987–415995, CSD-416088.

3. Results and discussion

3.1. Synthesis

The transition metal resources can be divalent metal acetate, chloride, sulfate, nitrate or oxalate. The reaction temperature and time are not exclusive which can alter from 180 to 240 °C and from 3 days to 2 weeks, respectively. The solid solution compounds of two different transition metals can be directly synthesized by using two transition metal salts in the reactions. Three crystals of such samples are structural characterized using single-crystal diffraction techniques (CSD-415993–415995). The crystallographic parameters are listed in Table 2. Others are confirmed by powder X-ray diffraction data, which are refined by Rietveld method using Topas [21,22] (Table 3). The ratios of two metal ions in products agree well with the starting ratios and the lattice constants of $(M_xM'_{x-1})$ compound are between M- and M'-compounds, respectively.

3.2. Structure description

The compounds $Na_2[M^{II}B_3P_2O_{11}(OH)]\cdot 0.67H_2O$ (M^{II} = Mg, Mn, Fe, Co, Ni, Cu, Zn) are all isostructural to each other, and crystallize in the space group $P6_3$. There are one unique M (M = Mg, Mn, Fe, Co, Ni, Cu, Zn) atom, three boron atoms, two phosphor atoms, eleven

Table 1
Crystallographic and structure refinement parameters for $Na_2[MB_3P_2O_{11}(OH)]\cdot 0.67H_2O$

M	Mg	Mn	Fe	Co	Ni	Cu	Zn
fw	369.68	400.31	401.22	404.30	404.08	408.91	410.74
Crystal system	Hexagonal	Hexagonal	Hexagonal	Hexagonal	Hexagonal	Hexagonal	Hexagonal
Space group	$P6_3$	$P6_3$	$P6_3$	$P6_3$	$P6_3$	$P6_3$	$P6_3$
Z	6	6	6	6	6	6	6
a (Å)	11.771(1)	11.940(2)	11.812(2)	11.759(2)	11.728(3)	11.554(2)	11.936(2)
c (Å)	12.100(1)	12.098(2)	12.067(2)	12.099(2)	12.074(1)	12.314(3)	12.363(3)
d_{calcd} (g cm^{-3})	2.537	2.670	2.742	2.781	2.799	2.862	2.683
F_000	1096	1174	1180	1186	1192	1198	1204
$R_1(I>2\delta(I))$[a]	0.0499	0.0423	0.0345	0.0392	0.0354	0.0391	0.0326
wR_2(all data)[a]	0.1525	0.1147	0.0998	0.1041	0.1229	0.1299	0.0897

[a] $R_1 = \sum(||F_0| - |F_c||)/\sum|F_0|$. w$R_2 = \left[\sum w(F_0^2 - F_c^2)^2/\sum w(F_0^2)^2\right]^{1/2}$. $w = 1/[\sigma^2(F_0^2) + (0.0497P)^2 + 11.5P]$, where $P = (F_0^2 + 2F_c^2)/3$.

Table 2
Crystallographic and structure refinement parameters for $Na_2[M_{1-x}M'_x B_3P_2O_{11}(OH)] \cdot 0.67H_2O$

$M_{1-x}M'_x$	$Co_{0.55}Ni_{0.45}$	$Co_{0.6}Zn_{0.4}$	$Mn_{0.47}Ni_{0.53}$
fw	404.20	406.87	402.31
Crystal system	Hexagonal	Hexagonal	Hexagonal
Space group	$P6_3$	$P6_3$	$P6_3$
Z	6	6	6
a (Å)	11.762(2)	11.746(2)	11.794(2)
c (Å)	12.115(2)	12.124(2)	12.074(2)
Cell volume (Å^3)	1451.5(4)	1448.6(4)	1454.5(4)
ρ_{cald} (g cm^{-3})	2.774	2.799	2.756
F_000	1189	1193	1184
$R_1(I>2\delta(I))$[a]	0.0450	0.0274	0.0700
wR_2 (all data)[a]	0.1425	0.0827	0.2046

[a] $R_1 = \sum(||F_0| - |F_c||)/\sum|F_0|$. $wR_2 = \left[\sum w(F_0^2 - F_c^2)^2/\sum w(F_0^2)^2\right]^{1/2}$. $w = 1/[\sigma^2(F_0^2) + (0.0497P)^2 + 11.5P]$, where $P = (F_0^2 + 2F_c^2)/3$.

Table 3
Refined results of cell lattice parameters of $Na_2[M_{1-x}M'_xB_3P_2O_{11}(OH)] \cdot 0.67H_2O$ in space group $P6_3$ (No. 173) from the powder X-ray diffraction data and x value from ICP analysis

$M_{1-x}M'_x$	x (Starting)	a (Å)	c (Å)	V (Å^3)	x (Product)
$Ni_{1-x}Mn_x$	0.50	11.838	12.091	1469.4	0.47
$Cu_{1-x}Mn_x$	0.50	11.736	12.238	1459.8	0.59
$Cu_{1-x}Mn_x$	0.67	11.838	12.201	1480.8	0.64
$Zn_{1-x}Mn_x$	0.50	11.850	12.128	1474.8	0.52
$Ni_{1-x}Co_x$	0.50	11.761	12.105	1450.0	0.55
$Zn_{1-x}Co_x$	0.50	11.751	12.128	1450.3	0.60
$Cu_{1-x}Ni_x$	0.50	11.646	12.211	1434.3	0.48
$Cu_{1-x}Ni_x$	0.75	11.702	12.142	1439.9	0.74
$Zn_{1-x}Ni_x$	0.50	11.736	12.111	1444.6	0.46
$Zn_{1-x}Cu_x$	0.50	11.647	12.250	1439.1	0.50

oxygen atoms and one −OH group in an asymmetric unit of the framework (Fig. 1). The boron atoms are presented both as BO_4 tetrahedra and $BO_2(OH)$ triangles, which are further linked forming three-member rings $B_3O_7(OH)$. The phosphor atoms are all located in regularly tetrahedral environment with the bond distances and angles range from 1.500(3) to 1.592(3) Å and from 103.59(19)° to 115.31(13)°, respectively. Here, the transition metal ions are distorted octahedral coordinated. In the MO_6 octahedra, four oxygen atoms in equatorial positions, belonging to the PO_4 tetrahedra, give four short bond distances from 1.969 to 2.180 Å, respectively. The axial positions are occupied by two oxygen atoms from the $B_3O_7(OH)$ groups, with two long bond distances from 2.212 to 2.384 Å. The M–O bond distances of seven compounds are listed in Table 4, which is in direct proportion to ionic radii. The distortion of MO_6 may partially originate from steric effect since both long M–O bonds are related to the bridged oxygen atoms which are rigidly bonded to two boron atoms. The steric effect can be evidenced by the Mg and Zn compounds, in which no d electron is involved in bonding.

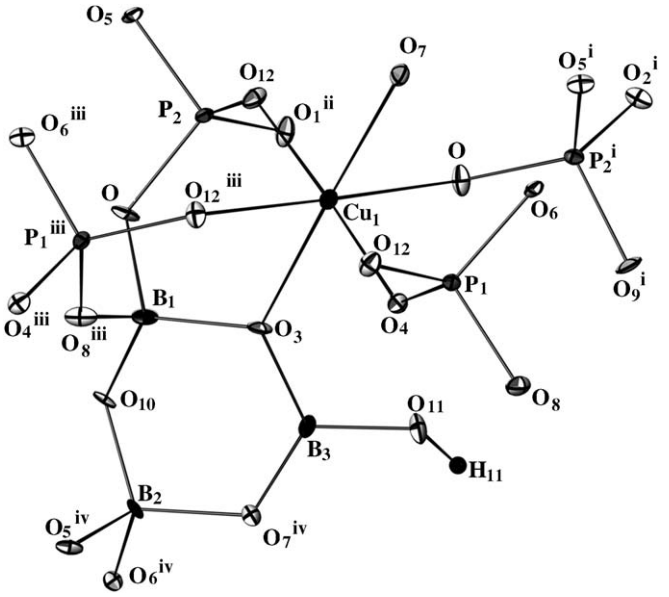

Fig. 1. ORTEP drawing (at 60% probability) of the coordination environment of copper atom in $Na_2[CuB_3P_2O_{11}(OH)] \cdot 0.67H_2O$. Symmetry codes: (i) $1-x+y$, $1-x$, z; (ii) $1-y$, $x-y$, z; (iii) $-x+y$, $1-x$, z and (iv) $1-x$, $1-y$, $1/2+z$.

Table 4
Bond lengths (Å) of M–O for $Na_2[MB_3P_2O_{11}(OH)] \cdot 0.67H_2O$ (M = Mg, Mn, Fe, Co, Ni, Cu, Zn)

M–O	Mg	Mn	Fe	Co	Ni	Cu	Zn
1[a]	2.019(2)	2.104(2)	2.061(2)	2.030(2)	2.014(2)	1.969(3)	2.055(2)
2	2.026(2)	2.129(2)	2.065(2)	2.038(2)	2.019(2)	1.971(3)	2.056(2)
3	2.028(2)	2.130(2)	2.068(2)	2.044(2)	2.049(2)	1.991(3)	2.074(2)
4	2.077(2)	2.180(2)	2.135(2)	2.110(2)	2.073(2)	1.992(3)	2.162(2)
5	2.229(3)	2.300(2)	2.245(2)	2.238(2)	2.212(2)	2.352(4)	2.299(2)
6	2.251(3)	2.306(2)	2.293(2)	2.293(3)	2.238(2)	2.384(4)	2.342(2)

[a]The bond lengths are listed in the order from the shortest to the longest.

However, one could also see the electronic influence on the geometry of the M octahedron. Transition metal ions, such as $Mn^{2+}(d^5)$, $Fe^{2+}(d^6)$, $Co^{2+}(d^7)$, $Ni^{2+}(d^8)$ and $Cu^{2+}(d^9)$, may have John–Teller effect but in different extent. The John–Teller effect is the strongest for Cu^{2+}, thus the Cu octahedron is significantly distorted with an averaged Cu–O difference of about 0.388 Å.

The open frameworks of the title compounds are composed of $B_3O_7(OH)$ groups and MP_2O_{10} layers formed by corner-sharing MO_6 and PO_4. Each MO_6 is surrounded by four PO_4 tetrahedra, which are further connected to other octahedra forming 6- and 12-membered windows paralleled along the ab plane (Fig. 2a). The layer can be considered as 4-connected plane net of (3^26^2) if only the sublattice of the transition metal atom is concerned. Such a plane net is a typical 2D Kagomé lattice, which may exhibit frustrated magnetic interaction as observed in a transition metal oxide $La_4Cu_2ZnMoO_{12}$ [23] when the M–M distance

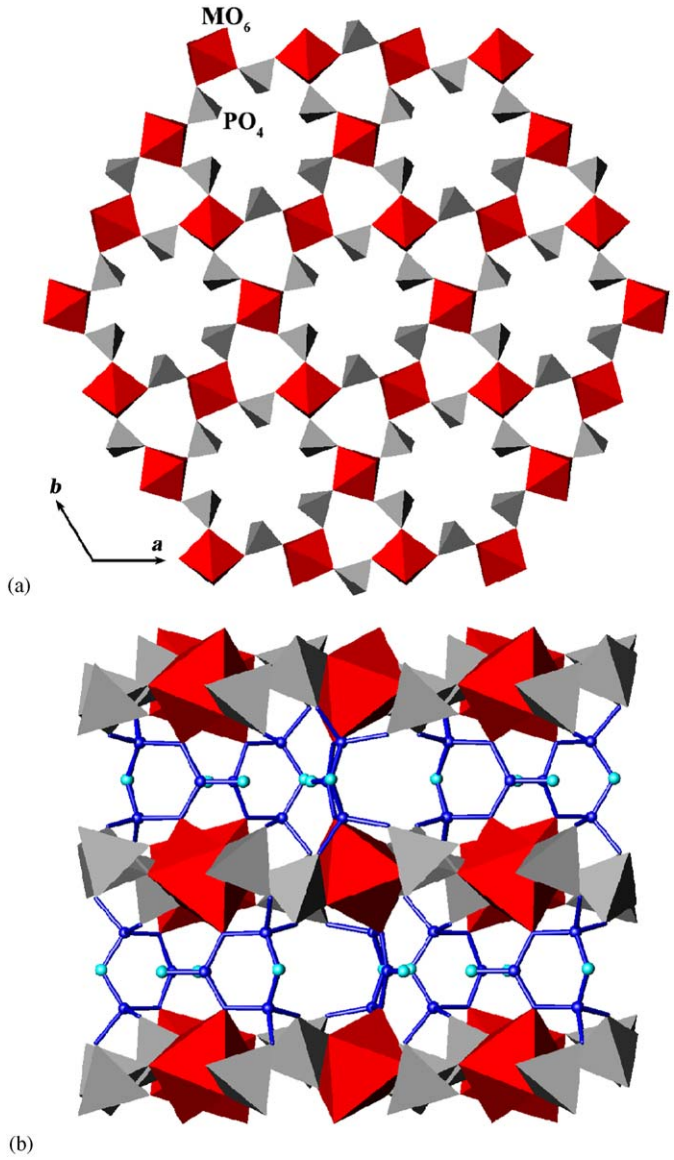

Fig. 2. (a) The MP_2O_{10} layer in $Na_2[MB_3P_2O_{11}(OH)]\cdot 0.67H_2O$; MO_6 octahedra: red, PO_4 tetrahedra: gray; (b) A projection of the $Na_2[M^{II}B_3P_2O_{11}(OH)]$ structure along the *a*-axis; MO_6 octahedra: red, PO_4 tetrahedra: gray; B atoms: blue balls, O atoms: sky-blue balls, B–O bonds: blue sticks. Na^+ ions and water molecules are omitted for clarity.

is short enough. However, within the layer, the *M*–*M* distance here is quite long (about 5.7 Å) and no obvious frustration is found (see the magnetic section below). The $B_3O_7(OH)$ group is a 3-membered ring consisting of two BO_4 and one $BO_2(OH)$ groups (according to bond valence sum (BVS) calculation, the terminal oxygen with BVS = 1.11 on the BO_3 group should bond to a proton as hydroxyl group). Although such 3-membered ring borate unit is common in borates, it is unusual in borophosphates particularly in those with 3D open framework structures. The four terminal oxygen atoms on BO_4 are shared with neighboring PO_4. In addition, two bridged oxygen atoms in the $B_3O_7(OH)$ are also shared with MO_6.

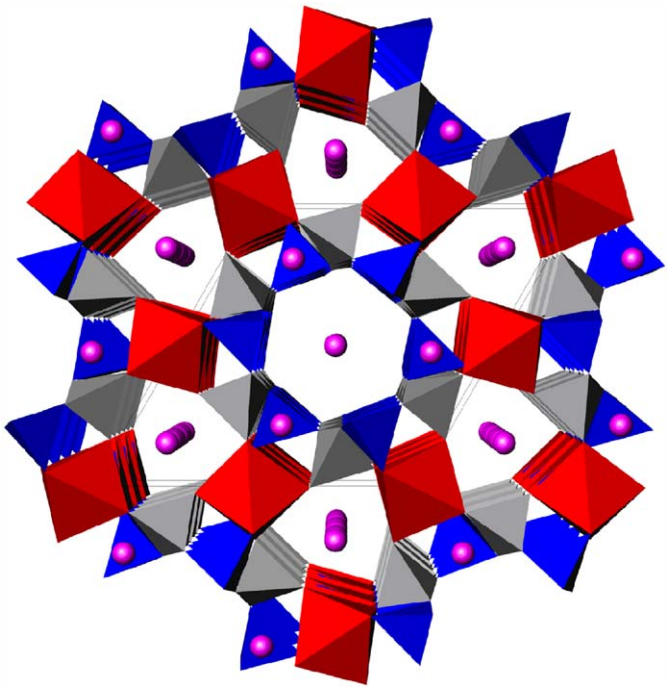

Fig. 3. A projection view of $Na_2[MB_3P_2O_{11}(OH)]\cdot 0.67H_2O$ along *c*-axis. Red octahedra: MO_6, blue tetrahedra and triangles: BO_4 and BO_3; gray tetrahedra: PO_4; balls: Na^+ and water molecules.

The 3D open framework can be considered as an alternative stacking of the MP_2O_{10} layer and the B_3O_8H groups along the *c*-axis (Fig. 2b). When the 3D open framework is projected along [001] direction, two kinds of channel can be found as shown in Fig. 3, one is stacked by the 12-membered rings formed by six MO_6 and six PO_4 corner-sharing alternatively, the other is stacked by 6-membered rings consisted of three MO_6 and three PO_4. Four distinct sodium cations, which compensate the negative charge of the framework, and some disengaged water molecules are presented in the channels and the voids of the structure. The sodium ions are irregularly coordinated by 6, 7 or 9 oxygen atoms with Na–O distance between 2.213 and 2.922 Å. Here in these structures, the atoms within the channels and the voids indicate strong ellipsoidal anisotropic phenomenon, which is due to the positional disorder of vibration.

3.3. Ion exchange and thermal stability

The counter Na^+ cations in the channels are mobile and can be exchanged by Li^+ in a melt of $LiNO_3$ at 285 °C without collapse of the framework expect for the Zn-compound. Table 5 lists the contents of Na^+ and Li^+ after 3 h exchange reaction. A large portion of the sodium ions in the as-synthesized samples can be replaced by lithium and, at the same time, the cell volumes reduce about 5% accompanied with the degression of crystallization. The Zn compound will be decomposed after this reaction.

Table 5
Structural parameters from powder X-ray diffraction refinement and the obtained Li^+:Na^+ molar ratio by ICP analysis for as-synthesized and ion-exchanged samples

Sample	As-synthesized			Ion-exchanged				
	a (Å)	c (Å)	v (Å^3)	a' (Å)	c' (Å)	V' (Å^3)	V'/V	Li^+:Na^+
Mg compound	11.794	12.114	1459.3	11.538	12.066	1391.1	95.3%	1.73:0.27
Mn compound	11.953	12.107	1498.0	11.710	11.997	1424.6	95.1%	1.58:0.42
Fe compound	11.845	12.114	1471.9	11.610	12.094	1411.8	95.9%	1.69:0.31
Co compound	11.754	12.117	1449.8	11.525	12.090	1390.7	95.9%	1.56:0.44
Ni compound	11.735	12.080	1440.7	11.461	12.041	1369.7	95.1%	1.59:0.41
Cu compound	11.556	12.352	1428.5	11.348	12.272	1368.6	95.8%	1.74:0.26

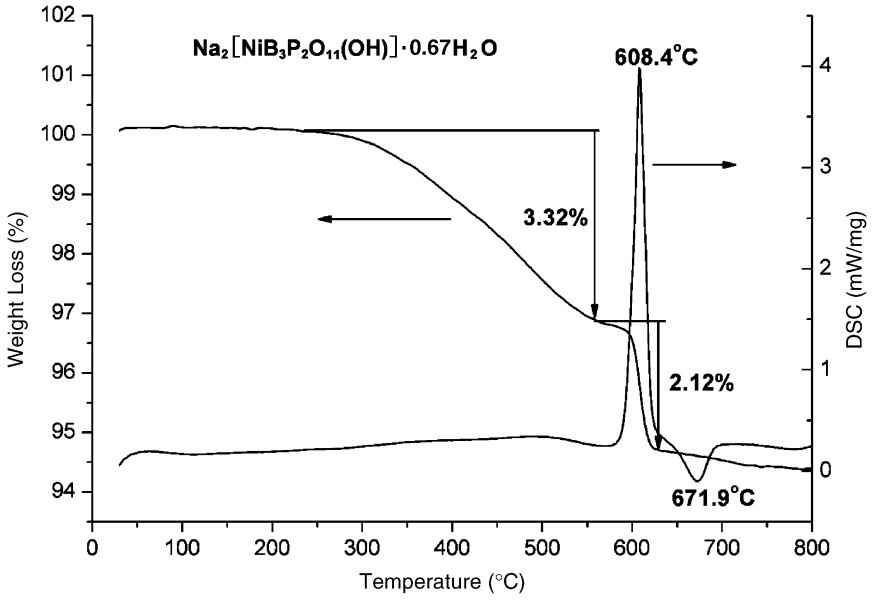

Fig. 4. The TGA and DSC curves of the as-synthesized Ni compound.

The as-synthesized samples lose weight stepwise as the increase of temperature in a similar way. Take $Na_2[NiB_3P_2O_{11}(OH)]\cdot 0.67H_2O$ as an example (Fig. 4), it gradually loses about 3.32 wt% up to 550 °C, originating from release of the water molecules in the channels, during which the framework retains but the cell volume decreases (see Fig. 5). At 608 °C, it shows a sharp weight loss (cal. 2.23% obs. 2.12%) and a heat absorption peak due to dehydration of the hydroxyl groups, which leads to collapse of the framework and formation of an amorphous product. The peak at 672 °C in DSC shows the sample melts. The as-synthesized Ni compound powder was heated at 25, 300, 400, 500, 550, 600 °C and cooled down to room temperature every step. The powder X-ray diffraction for that treated sample (Fig. 5) shows that the structure collapses beyond 550 °C, which is in agreement with the TGA and DSC curves. The frameworks of other analogs collapse between 500 and 550 °C (see the supplementary information).

3.4. Magnetic susceptibility

Fig. 6 shows the inverse of the magnetic susceptibility (χ^{-1}) as a function of temperature, for powdered $Na_2[M^{II}B_3P_2O_{11}(OH)]\cdot 0.67H_2O$ (M^{II} = Mn, Co, Ni, Cu). The curves follow the Curie–Weiss law from 20 to 140 K for all the four materials. The Weiss temperature (θ) and the Curie constant (C) are listed in Table 6. C value corresponds to an effective magnetic moment (M_{eff}), which is close to the spin-only value of M^{2+} ions. The deviation for the Co compound is largely due to its strong spin–orbital interaction. The Weiss temperature is negative in $Na_2[MB_3P_2O_{11}(OH)]\cdot 0.67H_2O$ (M = Mn, Co and Ni), indicating an antiferromagnetic ordering, and a ferromagnetic ordering is expected in $Na_2[CuB_3P_2O_{11}(OH)]\cdot 0.67H_2O$ with a positive θ. However, no magnetic phase transition is observed on cooling the samples to $T = 2$ K. The isothermal magnetization curves at $T = 2$ K are exhibited in Fig. 7. The magnetization curves depend

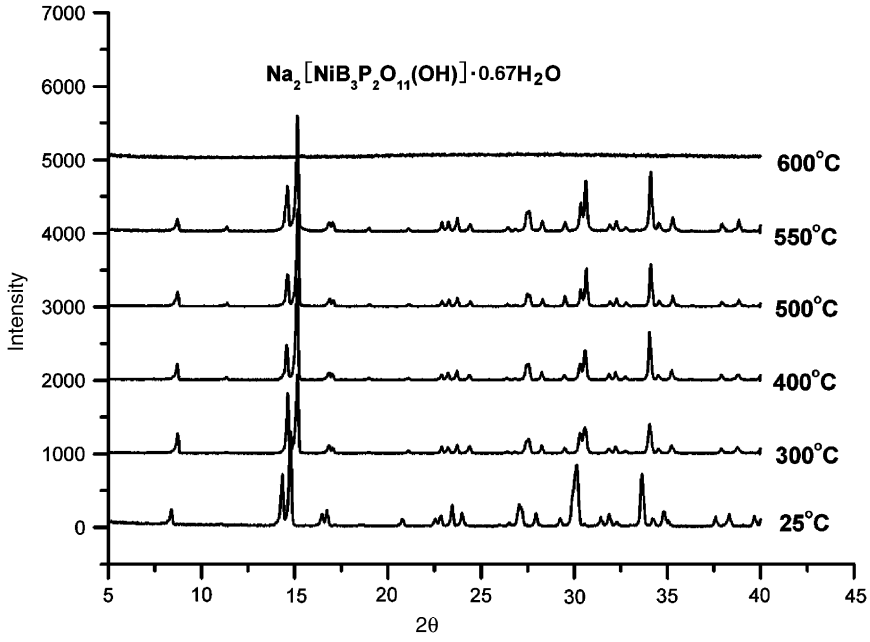

Fig. 5. X-ray diffraction patterns of $Na_2[NiB_3P_2O_{11}(OH)]\cdot 0.67H_2O$ treated at different temperatures.

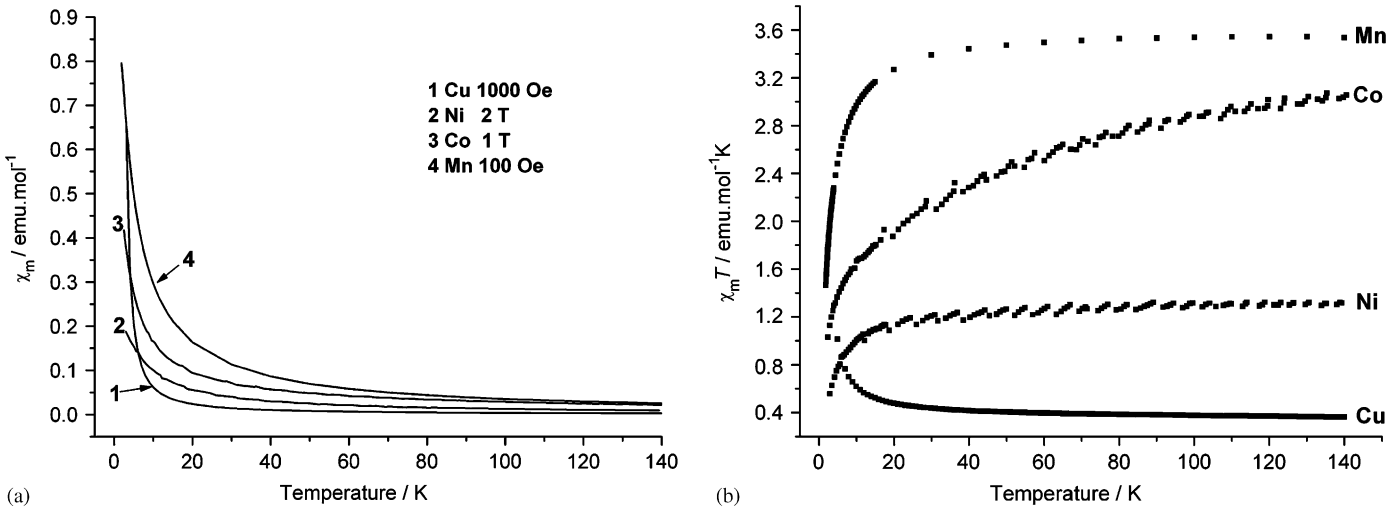

Fig. 6. χ_m (a) and $\chi_m T$ (b) vs. the temperature curves of $Na_2[MB_3P_2O_{11}(OH)]\cdot 0.67H_2O$ (M = Mn, Co, Ni and Cu)

Table 6
Magnetic parameters for $Na_2[M^{II}B_3P_2O_{11}(OH)]\cdot 0.67H_2O$ (M^{II} = Mn, Co, Ni and Cu)

M	θ (K)	C ($cm^3\,mol^{-1}\,K$)	M_{eff} (μ_B) experimental	M_{eff} (μ_B) spin-only value
Mn	−2.4	3.6	5.4	5.9
Co	−14.4	2.6	4.5	3.9
Ni	−3.0	1.2	3.1	2.8
Cu	10.0	0.34	1.6	1.7

strongly on H at low applied field, followed by saturation at high field. The magnetic moment at $H = 7$ T is $M = 1.6\,\mu_B$/Ni, $4.8\,\mu_B$/Mn, $2.3\,\mu_B$/Co and $0.98\,\mu_B$/Cu, respectively, coherent to $g\,\mu_B S$ for M^{2+} as expected. There appears a feature in these materials that the spins of the magnetic ions are aligned parallel easily by applied field, especially in the case of $Na_2[CuB_3P_2O_{11}(OH)]\cdot 0.67H_2O$, which reaches saturation at $H < 1$ T. As mentioned above, the MO_6 octahedra in $Na_2[MB_3P_2O_{11}(OH)]\cdot 0.67H_2O$ are isolated and well diluted by phosphate and borate groups with a nearest distance of 5.7 Å. The magnetic interaction would be expected to be rather weak. In addition, there is no obvious magnetic ordering even at low temperature as shown in Fig. 6. It is scarce to observe such an easy induction by moderately low applied field in such a dilute magnetic system. In other metal-rich borate systems such as $SrCu_2(BO_3)_2$, $Fe_3O_2BO_3$ and $Mn_2B_2O_5$[24–26], where magnetic metals are inside the oxygen octahedral or rectangular, sharing edges to form chains, ribbons or

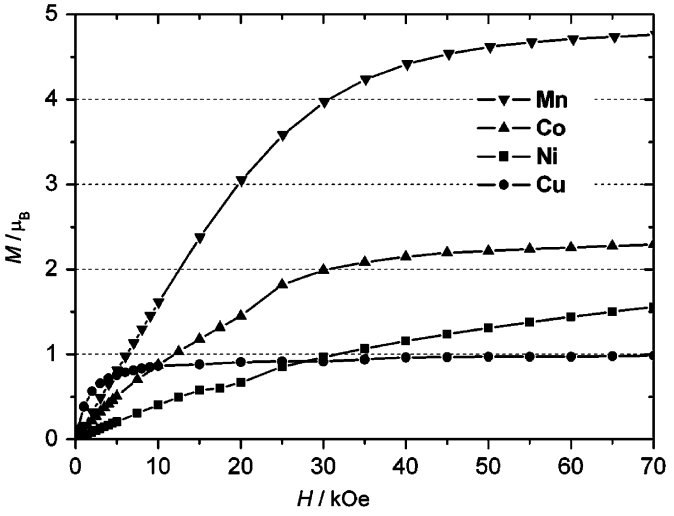

Fig. 7. The magnetization curves of $Na_2[MB_3P_2O_{11}(OH)]\cdot 0.67H_2O$ (M = Mn, Co, Ni and Cu) at 2 K.

dimer, the saturation is difficult to be induced even at high H. In $SrCu_2(BO_3)_2$, saturation is not able to be reached even at 40 T at 0.5 K. Compared with the metal-rich borates, phosphate and borate groups in $Na_2[MB_3P_2O_{11}(OH)]\cdot 0.67H_2O$ separate metals to a larger extent on one side, also provide diverse pathways between the magnetic ions.

4. Conclusions

$Na_2[M^{II}B_3P_2O_{11}(OH)]\cdot 0.67H_2O$ (M^{II} = Mg, Mn, Fe, Co, Ni, Cu, Zn) are hydrothermally synthesized and all crystallize in an open framework in the space group $P6_3$, which has mobile Na^+ cations located in the 12-membered ring channels. Their open frameworks are stable until 500 °C. Completed solid solutions of different transition metals can be obtained. The magnetic susceptibilities for $Na_2[M^{II}B_3P_2O_{11}(OH)]\cdot 0.67H_2O$ (M^{II} = Mn, Co, Ni, Cu) follow the Curie–Weiss law in a wide temperature range.

Acknowledgment

The project is supported by the National Nature Science Foundation of China (20221101) and (20471003).

Appendix A. Supplementary materials

Supplementary data associated with this article can be found in the online version at doi:10.1016/j.jssc.2006.04.052.

References

[1] R. Kniep, G. Gozel, B. Eisenmann, C. Rohr, M. Asbrand, M. Kizilyalli, Angew. Chem., Int. Ed. Engl. 33 (1994) 749–751.
[2] R. Kniep, H. Engelhardt, C. Hauf, Chem. Mater. 10 (1998) 2930–2934.
[3] R. Kniep, G. Schafer, H. Engelhardt, I. Boy, Angew. Chem. Int. Ed. 38 (1999) 3642–3644.
[4] I. Boy, F. Stowasser, G. Schafer, R. Kniep, Chem. Eur. J. 7 (2001) 834–839.
[5] R. Kniep, H.G. Will, C. Rohr, Angew. Chem., Int. Ed. 36 (1997) 1013–1014.
[6] A. Yilmaz, X. Bu, M. Kizilyalli, G.D. Stucky, Chem. Mater. 12 (2000) 3243–3245.
[7] S.C. Sevov, Angew. Chem., Int. Ed. Engl. 35 (1996) 2630–2632.
[8] G. Schafer, R. Kniep, Z. Anorg. Allg. Chem. 626 (2000) 141–147.
[9] G. Schafer, H. Borrmann, R. Kniep, Z. Anorg. Allg. Chem. 627 (2001) 61–67.
[10] R.P. Bontchev, A.J. Jacobson, Mater. Res. Bull. 37 (2002) 1997–2005.
[11] Y. Huang, G. Schafer, W. Carrillo-Cabrera, R. Cardoso, W. Schnelle, J.T. Zhao, R. Kniep, Chem. Mater. 13 (2001) 4348–4354.
[12] C.J. Warren, R.C. Haushalter, D.J. Rose, J. Zubieta, Chem. Mater. 9 (1997) 2694–2696.
[13] Y. Huang, G. Schafer, W. Carrillo-Cabrera, H. Borrmann, R. Gil, R. Kniep, Chem. Mater. 15 (2003) 4930.
[14] M. Wiebcke, A. Bögershausen, H. Koller, Micrpor. Mesopor. Mater. 78 (2005) 97–102.
[15] C. Hauf, R. Kniep, Z. Kristallogr. 211 (1996) 705–706.
[16] C. Hauf, R. Kniep, Z. Kristallogr. 211 (1996) 707–708.
[17] C. Hauf, R. Kniep, Z. Kristallogr, NCS 212 (1997) 313–314.
[18] I. Boy, R. Kniep, Z. Naturforsch. 54 (1999) 895–898.
[19] T. Higashi, ABSCOR, Empirical Absorption based on Fourier Series Approximation, Rigaku Corporation, Tokyo, 1995.
[20] [a] G.M. Sheldrick, SHELXS97, Program for Crystal Structure Solution, University of Göttingen, Göttingen, Germany, 1997;
[b] G.M. Sheldrick, SHELXL97, Program for Crystal Structure Refinement, University of Göttingen, Göttingen, Germany, 1997.
[21] H.M. Rietveld, J. Appl. Crystallogr. 2 (1969) 65–71.
[22] TOPAS V2.1, General Profile and Structure Analysis Software for Powder Diffraction Data; Bruker AXS, Karlsruhe, Germany.
[23] G.B. Li, L.P. You, W.T. Wei, Y. Lu, J. Ju, A. Wannberg, H. Rundlöf, X.D. Zou, T. Yang, Sh.J. Tian, F.H. Liao, N. Toyota, J.H. Lin, J. Am. Chem. Soc. 127 (2005) 14094–14097.
[24] H. Kageyama, K. Yoshimura, R. Stern, N. Mushnikov, K. Onizuka, M. Kato, K. Kosuge, C.P. Slichter, T. Goto, Y. Ueda, Phys. Rev. Lett. 82 (1999) 3168–3171.
[25] R.B. Guimaraes, M. Mir, J.C. Fernandes, M.A. Continentino, H.A. Borges, G. Cernicchiaro, M.B. Fontes, D.R.S. Candela, E. Baggio-Saitovitch, Phys. Rev. B 60 (1999) 6617–6622.
[26] J.C. Fernandes, F.S. Sarrat, R.B. Guimaraes, R.S. Freitas, M.A. Continentino, A.C. Doriguetto, Y.P. Mascarenhas, J. Ellena, E.E. Castellano, J.L. Tholence, J. Dumas, L. Ghivelder, Phys. Rev. B 67 (2003) 104413.